

Robust data management for high through-put light sheet microscopy of whole mouse brains

M. Caroline Müllenbroich,^{a,b} Ludovico Silvestri,^{a,c} Leonardo Onofri,^e Irene Costantini,^a Marcel Van t'Hoff,^f Leonardo Sacconi,^{a,c} Giulio Iannello,^e Francesco S. Pavone,^{a,b,c,d}

^aEuropean Laboratory for Non-linear Spectroscopy (LENS), University of Florence, Italy

^bDepartment of Physics and Astronomy, University of Florence, Italy

^cNational Institute of Optics, National Research Council, Italy

^dInternational Center for Computational Neurophotonics (ICON Foundation), Italy

^eIntegrated Research Centre, University Campus Bio-Medico of Rome, Italy

^fDistrio, Murmex

Abstract. 200 words limit. no numerical references presenting concisely the objectives, methodology used, results obtained, and their significance.

Keywords: Light sheet microscopy, big data, whole brain mounting, data management, whole brain imaging, rolling shutter, 7,8..

Address all correspondence to: First author, University Name, Faculty Group, Department, Street Address, City, Country, Postal Code; Tel: +1 555-555-5555; Fax: +1 555-555-5556; E-mail: myemail@university.edu

1 Introduction

The highly ambitious project of mapping and understanding each and every neuronal connection in the whole brain has been moved from the realm of wishful longing to feasible reality by the recent advent of light sheet fluorescent microscopy (LSFM). With this technique 3D data sets can be acquired with a resolution that is high enough to identify neurons and their dendritic, axonal and spine features in time scales which are no longer the bottle neck of high-throughput acquisition. In LSFM, the sample is illuminated with a thin sheet of light confined into the focal plane of the detection objective, which collects the fluorescence emission along an axis perpendicular to the illumination plane.¹ This technique drastically reduces the imaging acquisition time by recording millions of pixels in parallel and affords optical sectioning by operating fluorescence excitation and detection on separate, perpendicularly oriented paths where the excitation light sheet and the detection focal plane overlap (Figure 1,A). Consequently fluorophores outside the light sheet are neither bleached nor contribute blurring out-of-focus noise. Consequently LSFM reduces phototoxicity and photobleaching while achieving excellent resolution at high penetration depths; however, it requires the sample to be transparent.

Several challenges remain to be overcome, however, to allow fast and, most of all systematic, production of reliable datasets and their meaningful interpretation to further our understanding of neuronal networks. Those challenges include fast, cheap and reproducible sample preparation, automated image acquisition that does not require constant attention by an expert and, most crucially, the storage, interpretation and analysis of the unprecedented huge data sets light sheet microscopy routinely produces. The mapping and understanding of this “big data” is a colossal task that requires the expertise of computer scientists to employ fully automated post-processing, for example, to do cell counting or blood vessel segmentation. On the other hand, the imaging of large, intrinsically opaque samples in light sheet microscopy necessitates clearing protocols based

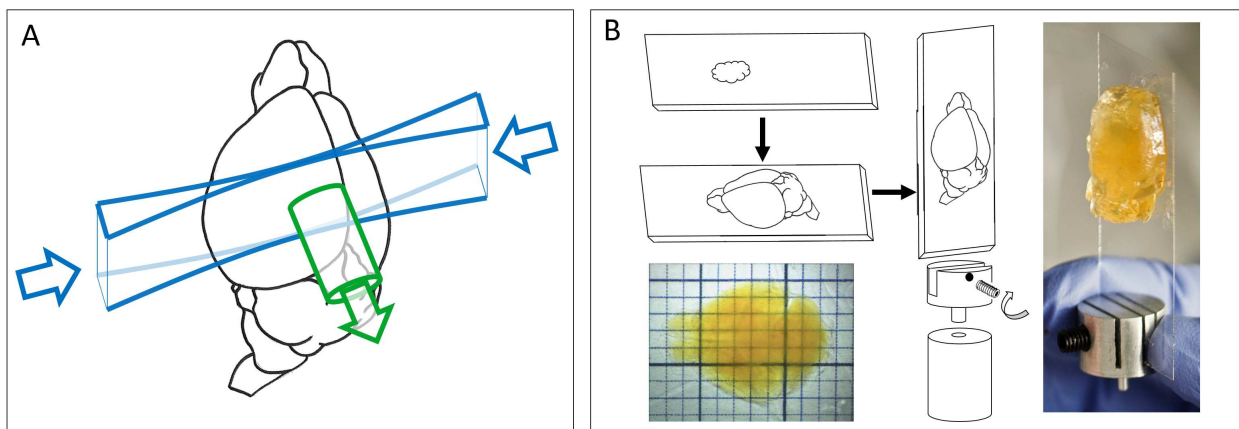


Fig 1: (A) Schematic of light sheet microscopy. The sample is illuminated with a planar light sheet (blue) perpendicular to fluorescence detection (green). (B) Mounting of a clarified, fluorescently labelled brain. The brain is glued onto a coverslip and inserted into an adapter that slides into a Teflon cylinder.

on refractive index matching which render the tissue transparent. This makes LSFM a truly interdisciplinary field in which the technological advances by optical developers need to be matched by novel development in the area of information and biotechnology.

Here we will present a state-of-the-art LSFM, as it is implemented in our lab, which is especially beneficial to acquire 3D data sets of large, clarified and structurally intact mouse brains. The LSFM features double-sided illumination with a digitally scanned light sheet and a sample chamber which has been specifically designed for the the imaging of large ($> 1\text{cm}^3$), immersed and freely movable samples. After briefly presenting the optical clearing protocol we employ to render our samples transparent, we explain how to prepare and mount the samples for stable, 3D imaging for several days. In addition to a full description of the optical setup, the control hardware and software, we further present a practical guide for the alignment of a LSFM, a non-trivial task that requires careful consideration. A systematic approach to handle, store and analyse the data is explained in detail. We further explain about the data volume we produce how it can be reduced and handled. The imaging capabilities are demonstrated by 3D reconstructions of biological specimens. The final sentence of the introduction needs to be amazing.

2 Sample mounting and motion

To elucidate neuronal projections and functional connections in structurally intact tissue it is paramount to be able to image centimeter-sized, clarified samples, such as mouse brains, with high resolution in whole mount preparation. While promising clearing protocols are well documented in literature,^{2,3} the question of sample preparation and mounting in light sheet microscopy is not trivial but requires novel approaches to such extent that it is becoming a separate field of research and very diverse strategies such as FEP tubes, 3D printed chambers and Quartz cuvettes have been reported,³⁻⁶ however, these approaches are limited to much smaller sample volumes. The problem of sample mounting in a light sheet microscope arises from the fact that optical access to the sample is required from 3-4 planar sides leaving only two opposing sides to insert, fix and move the sample. Most commonly the vertical direction is chosen. Stable mounting is hereby

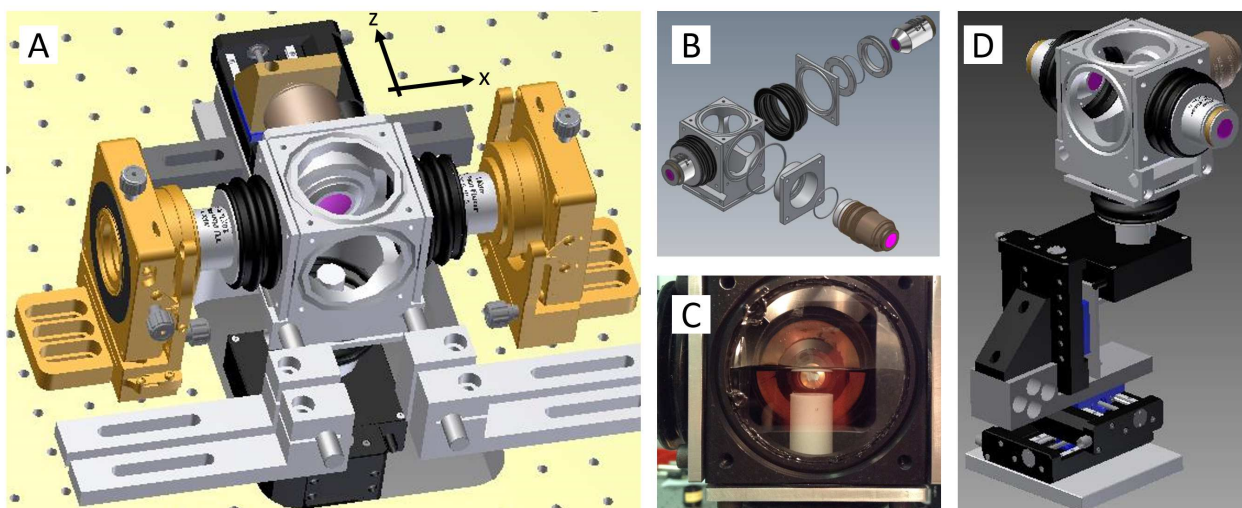


Fig 2: Schematic of light sheet microscopy. (A) Fluorescence excitation (along x axis) and detection (along z axis) are operated on independent, perpendicular light paths where the excitation light sheet and the detection focal plane overlap. The custom-made sample chamber is assembled with silicone bellows and seal rings. The clarified, fluorescently-labelled brain is mounted on a Teflon cylinder in the centre of the watertight chamber (C) and can be translated and rotated freely with piezo motors (D).

a key concern as a whole brain tomography can require image acquisition in excess of 24 hours and the effects of gravity, tissue shrinking/expansion and evaporation of the clearing solution over such time spans might have to be considered.

For the acquisition of whole brain data sets, we fix a clarified and fluorescently-labelled mouse brain with super glue to a coverslip (Figure 1,B). The brain is oriented along its axial orientation with the olfactory bulbs at the top and the cerebellum at the bottom of the coverslip. The coverslip is slid into a bottom adaptor and tightened with a plastic-capped grub screw. The bottom adaptor is inserted into a Teflon cylinder with the coverslip being positioned on the far side of the detection objective. Three different slits in the adapter correspond to varying distances to the detection objective and give variability in sample thickness for example to allow also for the mounting of rat brain hemispheres.

We designed a cubic, water-tight sample chamber (Figure 2,A) that allows access from all six sides while maintaining the 3D integrity of large, clarified and fluorescently-labelled mouse brains. The sample chamber is tightly bolted to the optical breadboard while soft connections using silicone bellows allow for adjustable movements of the objectives and free 3D motion of the motor stages (Figure 2,B). All connections are sealed with rubber rings and silicone caulk and additionally tightened with cable binders. In this way the objectives can be refocused and realigned without compromising the watertight seal of the chamber (Figure 2,C). The clarified brains are imaged immersed in clearing solution composed of 63% TDE in Phosphate buffered saline (PBS) and a refractive index of 1.45. To fill the entire volume of the sample chamber approximately 400ml clearing solution are needed. A motorized x-, y-, z-, θ -stage (Physik Instrumente, see Table 1) allows free 3D motion and rotation of the Teflon cylinder which reaches into the centre of the chamber (Figure 2,D). Illumination and detection axes are horizontal and the sampler rotation oc-

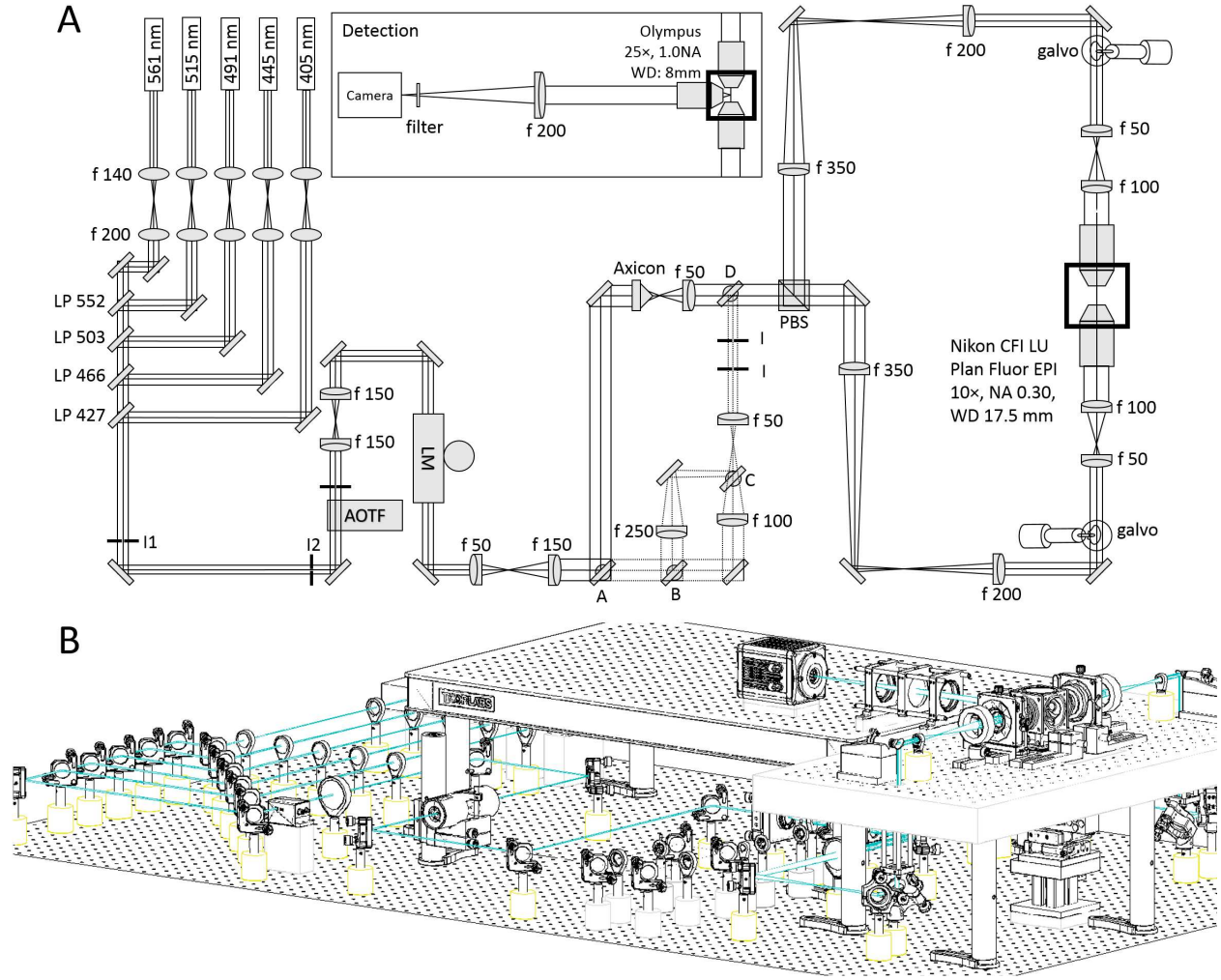


Fig 3: (A) Topview of the excitation path. The galvo scanners are mounted above periscopes. LP: long-pass filter, I: iris, AOTF: acousto-optical tunable filter, LM: laser modulator, PBS: polarisation beam splitter, ABCD: flip mirrors. Inset: detection. (B) Oblique view of the microscope. A custom-made breadboard serves to mount the sample chamber and objectives at an elevated height and features two circular holes at the edges for the periscopes and a large central cut out for the translation stages. A second breadboard is used for the camera.

curs around the vertical axis.

3 Optical path

3.1 Laser unit

The custom-made, confocal light sheet microscope is equipped with 5 linearly polarised, cw lasers for fluorescence excitation (Figure 3, A). The wavelengths were chosen to excite the most common fluorophores (see Table 1 for the manufacturer and specifications of opto-mechanical components). The laser light from each laser is first collimated and expanded with a telescope (f140, f200) and then combined into a common path with a beam steering mirror and a long-pass filter (Semrock,

LaserMUX™ series). An acousto-optical tunable filter (AOTF) acts as fast (μs) electronically tunable filter which uses the acousto-optical interaction inside an anisotropic medium to select and transmit any combination of up to four of the laser lines. The radio-frequency applied on the AOTF transducer controls the wavelength being transmitted into the first order and the radio-frequency amplitude allows to adjust the transmitted light intensity. Due its nonlinear response we measured the AOTF light transmittance for each wavelength as a function of radio frequency amplitude and determined a look-up table to linearise the output. The zero order light is blocked by an iris. An electro-optical laser modulator acts like a wave plate with electronically controlled retardation and rapidly rotates (few hundreds ns) the input polarisation of the excitation light by 90° . The wavelength-dependent, high voltage that needs to be applied to the birefringent crystal inside the modulator to change the optical path length is provided by a two-step pre-amplification system. First, a low voltage, analog signal from the DAQ board is pre-amplified with custom made electronics and then fed into a commercial high voltage amplifier. A digital line is used to electronically control the frequency with which the polarisation is changed. After the laser modulator the excitation beam is further expanded by a factor of two with two achromatic doublets (f100, f200).

3.2 *Illumination unit*

From here on three different light paths can be chosen through flip mirrors. One light path option guides the light through an axicon (apex angle of 160°) and an achromatic doublet (f50) to create a Bessel beam. The other two options create Gaussian beams of different beam diameter. This diameter variation translates to different fields of view later on in the detection path. The three options are recombined before a polarising beam splitter cube which splits the excitation light depending on its polarisation into one of the two identical excitation arms. The beam is reduced with a telescope (f350, f200) whose telecentric plane coincides with the mirrored surface of a galvanometric scanner (galvo). The galvos are mounted on a custom made optical breadboard which features two circular holes to pass the periscopic beams and a large central cut-out for the sample chamber and motor stages.

The scan mirror surface is re-imaged with a telescope (f50, f100) onto the back aperture of a long working distance, low magnification objective (Nikon, 10x 0.3NA WD 17.5mm). The two excitation objectives are designed for air immersion but are immersed into the clearing solution within the sample chamber. A coverslip glued to the front housing edge serves the dual purpose of maintaining the first diffractive surface between the front optical element and the air and to protect the front lens elements from the organic solvent. The light sheet is generated digitally^{7,8} by scanning the excitation beam across the focal plane of the detection objective. This generates incoherent illumination resulting in fewer artefacts. Additionally each line is specimen is illuminated with the same intensity creating a homogeneous light sheet which is particularly advantageous for the quantitative investigation of large samples in their entirety.

3.3 *Detection unit*

In it's simplest form, the fluorescence detection unit of a light sheet microscope is a conventional wide-field microscope: an objective lens, a fluorescent filter and a tube lens for an image on a wide-field detector. Fluorescence is collected with an objective that is specifically designed for immersion in clearing solutions. The objective is equipped with a correction collar allowing for immer-

sion in media with refractive indices ranging from 1.41 to 1.52 (Olympus, XLSLPLN25XGMP). To image the whole volume of interest the objective has a relatively low magnification of 25x and a large working distance of 8mm yet a high numerical aperture (1.0NA) affords high resolution imaging. A tube lens of 200mm creates the primary image on a sCMOS camera (Orca Flash4.0, Hamamatsu) with a chip of over 4 megapixels. In contrast to CCD sensors each pixel of a sCMOS camera sensor has a separate photodetector and amplification unit which means that sCMOS pixels can be read out independently from each other. The cell size of the OrcaFlash is $p^2 = 6.5\mu m \times 6.5\mu m$ over an active area of 13.3mm. With a 200mm tube lens the field of view in the sample is $480\mu m$.

In the rolling shutter data acquisition mode only a subset of adjacent horizontal pixel lines is simultaneously exposed and this active detection region is moved across the image sensor. With the delay between the exposure of two adjacent lines set to the minimum time required to read out a single line ($t = 9.7\mu s$, see Table2) the entire frame of 2048 horizontal lines is activated within 19.86ms. Setting the line exposure time to $l = 3ms$ results in approx. $k = l/t \approx 300$ lines being simultaneously exposed at any time. This detection area is swept from the top to the bottom of the chip and acts like a moving, virtual confocal slit corresponding to a width of $d_s = kp/M_{eff} = 0.72m$ in the sample space. With the given values of line exposure and line read out time, the camera acquires images at a frame rate of $\nu = 1/(2048t+l) \approx 44Hz$.

The camera was run as master in the internal trigger mode and a synchronisation pulse generated with the exposure of each new line was used as an output trigger for a data acquisition and generation device (DAQ) from National Instruments which was operated as slave. The saw-tooth driving signal for the galvo mirrors was generated by the DAQ and synchronised with the pixel line reset pulses from the camera to achieve confocal line detection.⁹ For optimal imaging it is crucial that the sample-emitted line of fluorescence is in the centre of the rolling shutter at the start of each image acquisition and furthermore travels with the same speed during stack acquisition. Any deviation from precise synchronisation results in image artefacts and severely degraded image contrast. The confocal resolution can be changed at run-time by changing the user-defined line exposure time and with it rolling shutter width, that is the number of horizontal pixel lines simultaneously exposed.

4 Optical characterisation

An overview of imaging properties and derived quantities is given in Table2.

4.1 Contrast

4.2 Signal-to-noise ratio

4.3 Optical sectioning

5 Alignment

For light sheet microscopy it is crucial that excitation and detection occur on perpendicular axes because any deviation from this geometry results in obscured images of reduced resolution and contrast. The objectives need to be perfectly confocal so that the fluorescence that is generated in the swept excitation beam also falls within the detection objective's focal plane. Telecentric imaging, that is the imaging with two lenses which are the sum of their focal lengths apart, a so-called 4f re-imaging system (Figure4,A), is used to re-image the galvo scanners onto the back apertures

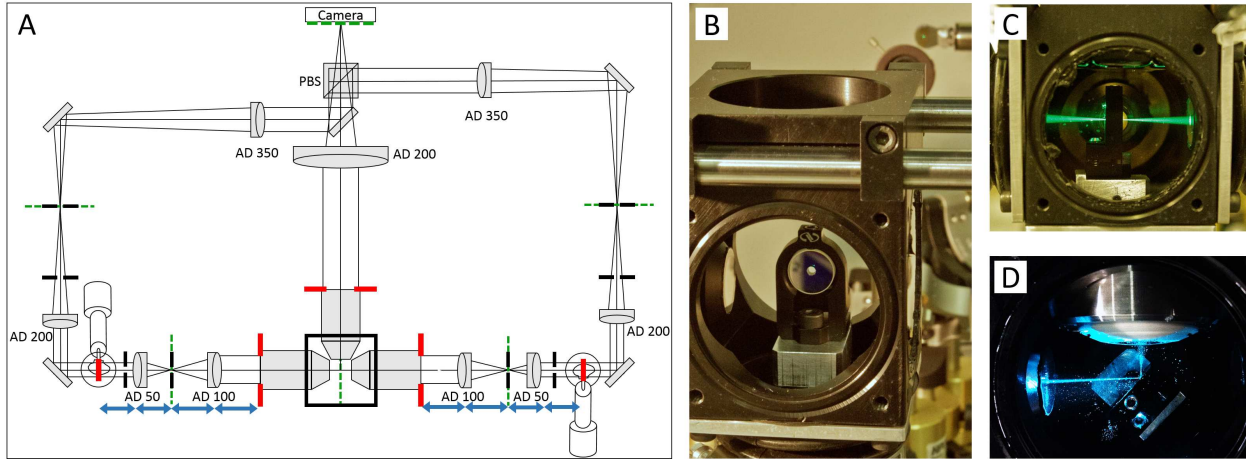


Fig 4: (A) Basic geometrical optics of a double-sided illumination light sheet microscope. AD: achromatic doublet, PBS: polarising beam splitter, red: objective back focal planes and conjugated telecentric planes, green: image planes, blue: 4f telecentric lens system, black: alignment irises. (B) Alignment mirror with drilled hole for light transmission, mount for tip adjustment and adaptor for the Teflon tube. (C) With lateral movement the alignment mirror can be placed such that light is transmitted into the opposing excitation arm. (D) The alignment mirror can be rotated to precisely reflect by 90° .

of the excitation objectives. In the detection path, the camera chip needs to be positioned in an image plane of the detection objective. Additionally, homogeneous illumination from both sides impose strict symmetry considerations on both illumination arms that have not only to be sufficiently aligned within themselves respectively but function as a pair with recursive dependence.

Our microscope was aligned with two tools, a shear plate to qualitatively assess collimation and a small mirror that can be mounted inside the sample chamber where the sample would usually be. The 0.5in mirror was first pierced with a drill using a ceramic drill bit to produce a hole roughly in its centre of the approximately the same diameter as the excitation beam inside the sample chamber (Figure 4,B). Using a compact single axis adjustable mirror mount (V50-AX, Newport) attached to the Teflon cylinder inside the chamber allows to adjust the pitch of the reflection with the mount and the yaw with the rotation stage while at the same time providing a very space efficient mounting for the pierced 0.5in mirror. With this “sample mirror” three different position can be easily implemented, firstly, back reflection by hitting the reflective surface at 0° , secondly, transmission by laterally displacing the mirror until the light passes through the drilled hole (Figure 4,C), and thirdly, reflection of the light by 90° by precisely turning the mirror mount by 45° using the rotation stage (Figure 4,D).

The excitation objectives are fixed on mounts which allow three dimensional translation plus pitch and yaw adjustment (LP-1A, Newport). In a first alignment step the beam paths of both excitation arms were brought to overlap through irises placed on the breadboard and the optical bench without any microscope objectives. We found it useful to use two mirrors in each periscope, one vertically mounted and one mounted at 45° for vertical deflection of the incoming beam. In this way full beam steering can be achieved to realign the periscope before hitting the galvo scanner. After this initial alignment the sample mirror was placed with its reflective surface in the centre

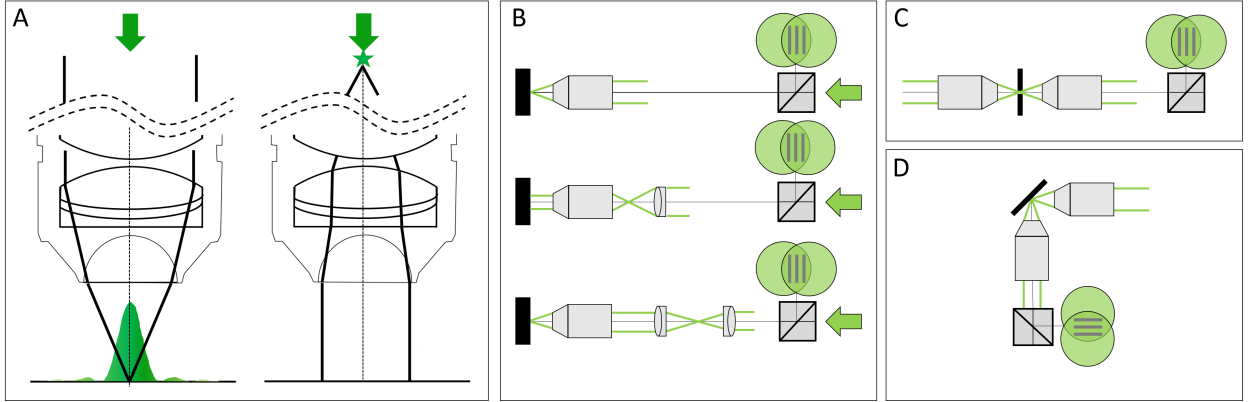


Fig 5: (A) Working principle of a microscope objective (left): a collimated input beam is converted into a spherical wavefront. Right: inverted light path, a focal spot in the back aperture creates a collimated output. (B) Recursive placement of lenses using the sample mirror in back-reflection mode, (C) in transmission mode and (D) in reflection mode.

of the central cut-out of the breadboard. The first excitation objective was placed into the beam path and brought to focus onto the sample mirror which was adjusted to reflect the light back into the same objective through the irises. Using a shear plate and a beam splitter cube the back reflected light was qualitatively adjusted for collimation using translation along the excitation axis of the objective mount (Figure 5, B). The sample mirror was then moved laterally to allow the excitation beam to pass through the drilled hole and the second excitation objective was placed (Figure 5, C). This time collimation was checked with the light going through both objectives and so their confocal placement was insured. Both excitation arms were then aligned recursively by starting at the putative confocal point between the objectives and placing successively lens after lens in the direction towards the light source, alternating between the two modalities illustrated in Figure 5, A. Finally, the sample mirror was positioned in deflection mode and the detection objective was aligned (Figure 5, D).

6 Data

Everybody take a look at Figure 6 because it is the best we have.

7 Conclusion

summary Light sheet microscopy has already been a game changer for large-scale imaging by yielding data with a combination of unprecedented spatio-temporal scale. The impact of this unique measurement technique will continue to revolutionise the field of whole brain connectomics due to its ability to record millions of images over the course of days or even weeks. The data produced in this fashion easily amounts several TB per data set and needs to be stored, transferred, retrieved, processed and visualised necessitating the concurrent development of novel computational interface and analysis methods. The latter need to be robust, standardised and fully automated processes yet allow for flexible, exploratory and tailored analysis.

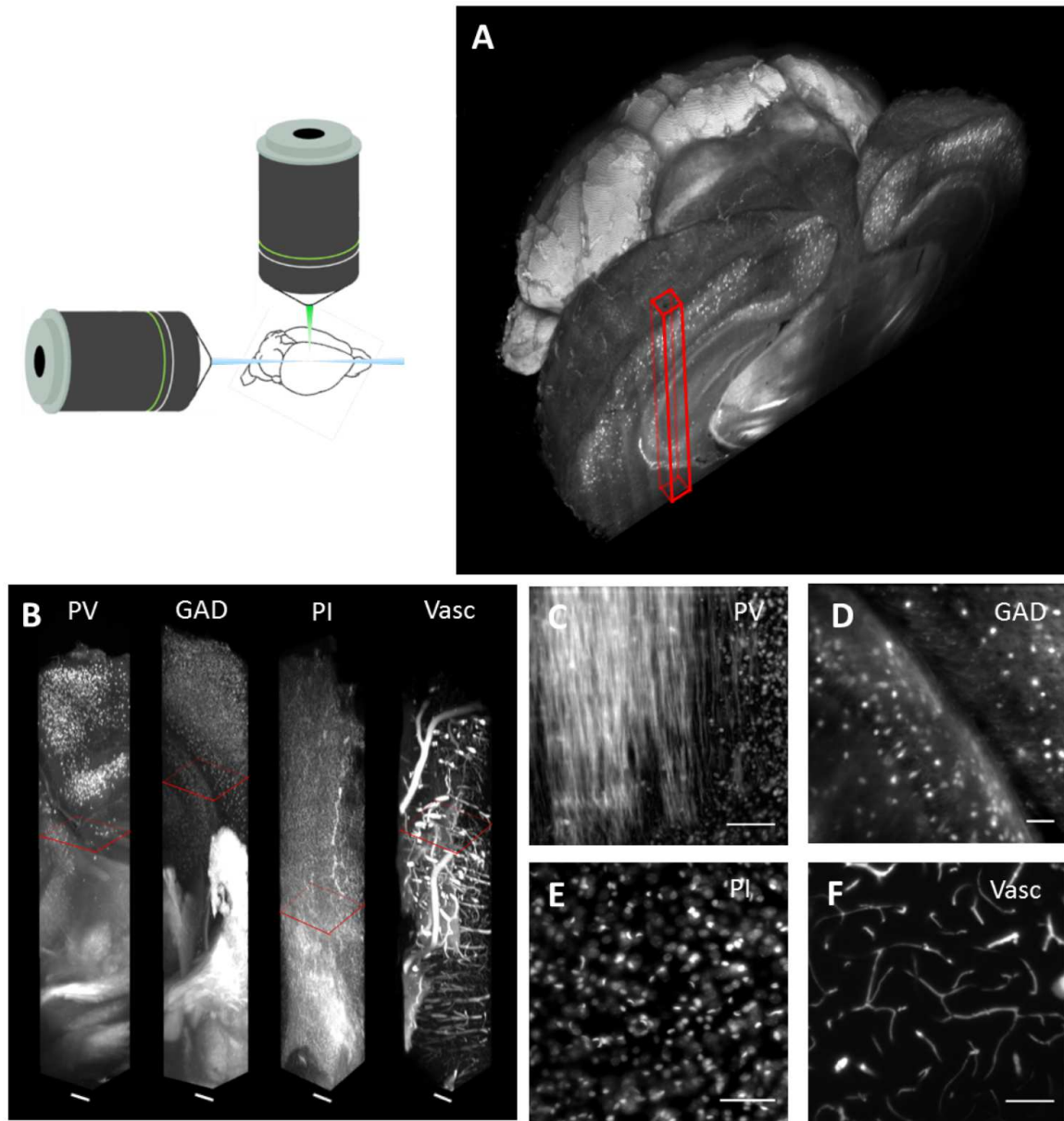


Fig 6: Whole mouse brain tomography. Imaging of whole transgenic mouse brains treated with CLARITY and cleared with TDE 63% imaged with LSM (Olympus, 25X objective). (A) 3D rendering of a parvalbumin-dTomato brain. (B) 3D rendering of stacks from PV-dTomato mouse brain, GAD-dTomato mouse brain, PI stained mouse brain, FITC-albumin labeled mouse brain, scale bar = 400 m. (C,D,E,F) High resolution insert, of the stack corresponding to red boxes in C. Scale bar = 100 m.

8 Outlook

where are we going next with this? ask Leo Onofri and Giulio to contribute to this, issues data mangament, aberration correction mapping of complementary data sets obtained in the same system, eg structural connectivity, morphology and gene expression.

Table 1: Overview of optomechanical components.

Component	Manufacturer	Part#	Specifications
Lasers	Cobolt AB, Sweden	MLD	405nm (for DAPI), 80mW, s-polarised
		MLD	445nm (for CFP), 50mW, s-polarised
		Calypso	491nm (for GFP, FITC), 50mW, s-polarised
		Fandango	515nm (for Venus, YFP), 50mW, s-polarised
		Jive	561nm (for dTomato, PI, RFP), 50mW, s-polarised
AOFT	AA Opto-Electronic, France	AOTFnC-400.650-TN	> 90% diffraction efficiency, 3nm resolution, low cross talk between laser lines, high separation angle
Laser modulator	Qioptiq GmbH, Germany	LM 0202 VIS ADP	400-650nm , $\lambda/2$ -voltage (633nm): 210V
Pulse amplifier	Falco Systems, The Netherlands	WMA-300	50x amplification up to ± 150 V, DC to 5MHz signal bandwidth
Galvo scanner	Cambridge Technology, USA	6220H	small angle step response $200\mu s$
Objectives	Nikon; Japan	Plan Fluor EPI	10x0.3NA, WD 17.5mm, EFL 20mm (excitation)
	Olympus, Japan	LMPLFLN20X	20x0.4NA, WD 12mm, EFL 9mm (detection)
Motor stages	Physik Instrumente, Germany	C-863.11	DC servo-motor controller
		M-122	Travel range 25mm, $0.1\mu m$ resolution, max. velocity 20mm/s
		M-116	Precision Rotation Stage, $2.5\mu rad$, max. velocity $20^\circ/s$
Camera	Hamamatsu, Japan	Orca Flash4.0	sCMOS sensor, 2048(H) x 2048(V), cell dim.: $6.5\mu m$, active area: 13.3mm x 13.3mm, 16bit images
DAQ board	National Instruments, USA	NI PCIe-6353	AI: 1 MS/s multichannel; 16-bit resolution, 10 V; AO: 2.86 MS/s, 16-bit resolution, 10 V; digital I/O lines (hardware-timed up to 10 MHz), 100MHz max counter frequency
Workstation	Dell, USA	T7500	12GB RAM, Intel Xeon Processor X5647 @ 2.93 GHz, 64bit OS, Win7

Table 2: Imaging properties and derived quantities. The thickness of the light sheet is approximately of the same size as the depth of field of the high NA detection lens.

Detection			
wavelength	λ	0.5	μm
refractive index	n	1.45	
numerical aperture	NA_d	1	
magnification	$M_{\text{eff}} = f_{\text{TL}}/\text{EFL}$	27.8	
tube lens	f_{TL}	200	mm
effective focal length objective	$\text{EFL} = f_{\text{TL}}/M$	7.2	mm
diameter back focal plane	$\text{BFP} = 2 \cdot \text{EFL} \cdot NA_d$	14.4	mm
field number	FN	18	mm
field size in specimen	$S = \text{FN}/M$	0.65	mm
depth of field	$\Delta = \lambda \cdot n / (NA_d)^2 + n \cdot e / M \cdot NA_d$	1.06	μm
Airy radius lat.	$r_A = 0.61\lambda / NA_d$	0.31	μm
Excitation			
numerical aperture	NA_e	0.3	
magnification, nominal	m	10	
tube lens	f_{tl}	100	mm
effective focal length, objective	$\text{efl} = f_{\text{tl}}/m$	20	mm
magnification, effective	$m_e = f_{\text{tl}}/\text{efl}$	5	
refractive index	η	1	
beam radius	ω	4.5	mm
min light sheet waist	$\omega_0 = \lambda \text{efl} / \pi \omega$	1.41	μm
confocal parameter	$b = 2\pi\omega_0^2/\lambda$	25.15	μm
Camera			
cell size	e	6.5	μm
effective area	r^2	13.3 ²	mm^2
line read out time	t	9.7	μs
line exposure time	l	3	ms
slit width, camera space	$d_c = l \cdot e / t$	2	mm
slit width, sample space	$d_s = d_c / M$	0.72	mm
frame rate	$\nu = 1/(2048 \cdot t + l)$	43.6	Hz

Acknowledgments

workshop boys cause they are amazing. Human Brain Project tutta la vita. GARR gave us a beautiful 10gb fiber to cineca CINECA for hosting us on pico

References

- 1 J. Huisken and D. Y. Stainier, “Selective plane illumination microscopy techniques in developmental biology,” *Development* **136**(12), 1963-1975 (2009). [1](#)
- 2 K. Chung, J. Wallace, S. Y. Kim, S. Kalyanasundaram, A. S. Andalman, T. J. Davidson and K. Deisseroth, “Structural and molecular interrogation of intact biological systems,” *Nature* **497**(7449), 332-333 (2013). [2](#)
- 3 R. Tomer, L. Ye, B. Hsueh and K. Deisseroth, “Advanced CLARITY for rapid and high-resolution imaging of intact tissues,” *nature protocols* **9**(7), 1682-1697 (2014). [2](#)
- 4 A. Kaufmann, M. Mickoleit, M. Weber and J. Huisken, “Multilayer mounting enables long-term imaging of zebrafish development in a light sheet microscope,” *Development* **139**(17), 3242-3247 (2012). [2](#)
- 5 P. Pitrone, J. Schindelin, L. Stuyvenberg, S. Preibisch, M. Weber, K. W. Eliceiri, J. Huisken and P. Tomancak, “OpenSPIM—an open access platform for light sheet microscopy,” *arXiv preprint arXiv:1302.1987*, 3242-3247 (2013). [2](#)
- 6 O. E. Olarte, J. Licea-Rodriguez, J. A. Palero, E. J. Gualda, D. Artigas, J. Mayer and P. Loza-Alvarez, “Image formation by linear and nonlinear digital scanned light-sheet fluorescence microscopy with Gaussian and Bessel beam profiles,” *Biomedical optics express* **3**(7), 1492-1505 (2012). [2](#)
- 7 P. J. Keller and E. H. K. Stelzer, “Quantitative in vivo imaging of entire embryos with digital scanned laser light sheet fluorescence microscopy,” *curr. Opin. Neurobiol.* **18**(6), 624-632 (2008). [5](#)
- 8 P. J. Keller, A. D. Schmidt, J. Wittbrodt, and E. H. K. Stelzer, “Reconstruction of zebrafish early embryonic development by scanned light sheet microscopy,” *Sciences* **322**(5904), 1065-1069 (2010). [5](#)
- 9 E. Baumgart and U. Kubitschek, “Scanned light sheet microscopy with confocal slit detection,” *Optics express* **20**(19), 21805-21814 (2012). [6](#)
- 10 L. Silvestri, A. Bria, L. Sacconi, G. Iannello, and F. S. Pavone, “Confocal light sheet microscopy: micron-scale neuroanatomy of the entire mouse brain,” *Opt Express* **20**(18), 20582-20598 (2012).
- 11 P. Frasconi, L. Silvestri, P. Soda, R. L. Cortini, F. S. Pavone and G. Iannello, “” *Bioinformatics* **30**(), i587-i593 (2014).
- 12 A. Bria and G. Iannello, “TeraStitcher-A tool for fast automatic 3D-stitching of teravoxel-sized microscopy images,” *BMC bioinformatics* **13**(1), 316 (2012).

List of Figures

- 1 (A) Schematic of light sheet microscopy. The sample is illuminated with a planar light sheet (blue) perpendicular to fluorescence detection (green). (B) Mounting of a clarified, fluorescently labelled brain. The brain is glued onto a coverslip and inserted into an adapter that slides into a Teflon cylinder.
- 2 Schematic of light sheet microscopy. (A) Fluorescence excitation (along x axis) and detection (along z axis) are operated on independent, perpendicular light paths where the excitation light sheet and the detection focal plane overlap. The custom-made sample chamber is assembled with silicone bellows and seal rings. The clarified, fluorescently-labelled brain is mounted on a Teflon cylinder in the centre of the watertight chamber (C) and can be translated and rotated freely with piezo motors (D).
- 3 (A) Topview of the excitation path. The galvo scanners are mounted above periscopes. LP: long-pass filter, I: iris, AOTF: acousto-optical tunable filter, LM: laser modulator, PBS: polarisation beam splitter, ABCD: flip mirrors. Inset: detection. (B) Oblique view of the microscope. A custom-made breadboard serves to mount the sample chamber and objectives at an elevated height and features two circular holes at the edges for the periscopes and a large central cut out for the translation stages. A second breadboard is used for the camera.
- 4 (A) Basic geometrical optics of a double-sided illumination light sheet microscope. AD: achromatic doublet, PBS: polarising beam splitter, red: objective back focal planes and conjugated telecentric planes, green: image planes, blue: 4f telecentric lens system, black: alignment irises. (B) Alignment mirror with drilled hole for light transmission, mount for tip adjustment and adaptor for the Teflon tube. (C) With lateral movement the alignment mirror can be placed such that light is transmitted into the opposing excitation arm. (D) The alignment mirror can be rotated to precisely reflect by 90° .
- 5 (A) Working principle of a microscope objective (left): a collimated input beam is converted into a spherical wavefront. Right: inverted light path, a focal spot in the back aperture creates a collimated output. (B) Recursive placement of lenses using the sample mirror in back-reflection mode, (C) in transmission mode and (D) in reflection mode.
- 6 Whole mouse brain tomography. Imaging of whole transgenic mouse brains treated with CLARITY and cleared with TDE 63% imaged with LSM (Olympus, 25X objective). (A) 3D rendering of a parvalbumin-dTomato brain. (B) 3D rendering of stacks from PV-dTomato mouse brain, GAD-dTomato mouse brain, PI stained mouse brain, FITC-albumin labeled mouse brain, scale bar = 400 μ m. (C,D,E,F) High resolution insert, of the stack corresponding to red boxes in C. Scale bar = 100 μ m.

List of Tables

- 1 Optomechanics
- 2 Resolution